

Annual Review of Physical Chemistry
**Hydration Mimicry by
 Membrane Ion Channels**

Mangesh I. Chaudhari,¹ Juan M. Vanegas,^{1,2} L.R. Pratt,³
 Ajay Muralidharan,^{3,4} and Susan B. Rempe¹

¹Department of Computational Biology and Biophysics, Sandia National Laboratories, Albuquerque, New Mexico 87185, USA; email: slrempe@sandia.gov

²Current affiliation: Department of Physics, University of Vermont, Burlington, Vermont 05405, USA

³Department of Chemical and Biomolecular Engineering, Tulane University, New Orleans, Louisiana 70118, USA

⁴Current affiliation: Department of Chemistry, University of Wisconsin, Madison, Wisconsin 53706, USA

Annu. Rev. Phys. Chem. 2020. 71:461–84

First published as a Review in Advance on
 March 9, 2020

The *Annual Review of Physical Chemistry* is online at
physchem.annualreviews.org

<https://doi.org/10.1146/annurev-physchem-012320-015457>

Copyright © 2020 by Annual Reviews.
 All rights reserved

**ANNUAL
 REVIEWS CONNECT**

www.annualreviews.org

- Download figures
- Navigate cited references
- Keyword search
- Explore related articles
- Share via email or social media

Keywords

biomolecular hydration mimicry, membrane ion channels, hydration of metal ions, hydration free energy, quasi-chemical theory, KcsA, MgtE, Ca_vAb

Abstract

Ions transiting biomembranes might pass readily from water through ion-specific membrane proteins if these protein channels provide environments similar to the aqueous solution hydration environment. Indeed, bulk aqueous solution is an important reference condition for the ion permeation process. Assessment of this hydration mimicry concept depends on understanding the hydration structure and free energies of metal ions in water in order to provide a comparison for the membrane channel environment. To refine these considerations, we review local hydration structures of ions in bulk water and the molecular quasi-chemical theory that provides hydration free energies. In doing so, we note some current views of ion binding to membrane channels and suggest new physical chemical calculations and experiments that might further clarify the hydration mimicry concept.

1. BACKGROUND

Cells control salt concentration differences across boundary membranes by transporting ions selectively (1). Selective ion transport plays an important role in numerous physiological functions, including electrical signaling and cell volume control. To that end, proteins—either channels or transporters—provide pathways for ions to permeate. Blocking such pathways can have either beneficial or detrimental effects. In beneficial cases, drugs that block specific channels hold promise for treating neurological disorders, autoimmune diseases, and cancers (2–4). Peptide toxins from several poisonous animals are examples of detrimental possibilities (5, 6). Indeed, simple divalent metal ions can be potent channel blockers, and both monovalent and divalent ions permeate selectively. In addition to their important roles in health, cellular mechanisms of ion transport can also guide materials science by inspiring (7, 8), or being integrated into (9, 10), synthetic membranes for efficient power generation, water purification, mineral recovery, and separation of small molecules from mixtures (11).

According to a concept called hydration mimicry, ions might pass easily from water through protein channels when pore-lining amino acid residues arrange a local environment that mimics the local ion hydration environment (12–15). Here, local structure refers to atoms that interact with an ion, making direct contacts. That local structural similarity may lead to a free energy for ion binding that approximately equals the free energy for ion hydration in bulk liquid water, with moderate barriers leading to rapid ion permeation (**Figure 1**).

Similarly, other ions may encounter large free energy barriers, leading to rejection from the protein pore if a binding site offers a poor hydration mimic (**Figure 1**). Alternatively, an ion may be trapped by binding too strongly to a channel (**Figure 1**) and thus block passage of a native permeant ion (16–20).

Primitive concepts for the design of biomimetic transport (21, 22) may begin with a focus on the direct contacts of an ion in transit and on the consequences for the binding free energies. Contacts should be chemically competent for binding that is satisfactory but not too strong (23). Those binding contacts should be available and sufficiently flexible to accommodate ions in satisfactory binding geometries. Binding geometries may be characterized by properties such as the number of contacts, or coordination number, and the distance between an ion and its contacts, or cavity size. Binding geometries may also be constrained by properties of the binding sites, such as covalent bonds, or by interactions with the proximal environment. Longer-range interactions, electrostatic

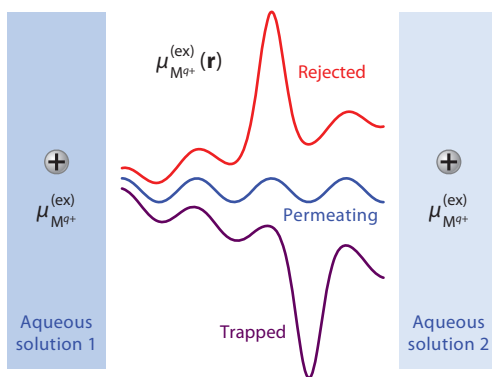


Figure 1

Do ion channels mimic the aqueous hydration of ions that readily permeate? Hypothetical molecular-scale variation of the free energies of ion binding, $\mu_{M^{q+}}^{(ex)}(r)$, illustrates rejected, permeating, and trapped cases.

and dispersive, are also essential but perhaps not decisive in comparing ions with the same charge and similar sizes. Few approaches can treat all of these features. Fortunately, a recent statistical thermodynamic theory—quasi-chemical theory (QCT)—offers a descriptive tool that facilitates analysis of those primitive structural concepts and their effect on ion binding free energies. QCT is a feature of the remainder of this review.

It is tempting to go further with refined hydration mimicry concepts, say, by noting interesting higher-resolution details of ion–protein binding configurations. But such comparisons have been limited by lack of the corresponding higher-resolution characterization of the binding of relevant ions to the bulk solution, which defines the end points of ion transfer. Elucidating the details of natural bulk ion hydration has been a challenge (24–27). Here, we collect and discuss important results from recent research.

Theoretical studies (28–30) that assess the structure–free energy relationship between an ion and the protein it binds to, relative to binding in water, are rarer than direct numerical simulations of such systems despite an abundance of high-resolution cryo-electron microscopy and crystal structures for channels and transporters (12, 13, 31–37). Here, we analyze the hydration mimicry concept by comparing local structure exhibited by molecular simulations of ion hydration with crystal structures of ion binding sites in channels and transporters. We also connect local hydration structure with the free energy of ion binding to water. Our results emphasize the importance of coordination number and of neighborhood analyses of molecular simulations in order to characterize local ion hydration structure, thus permitting comparison with experimental data on local structure for ions in channel and transporter binding sites. Neighborhood analyses also enhance the utility of the QCT for testing the hydration mimicry idea. Altogether, our results demonstrate unexpected relationships between local solvent structure and transfer free energies for ion permeation, rejection, and trapping that support an expanded view of hydration mimicry.

1.1. Ions in Water

Water is the reference environment for ion transport across cellular membranes. Transport takes ions from one aqueous solution to another, and may bring water molecules along as well (1, 38–41). Since protein channels and transporters catalyze ion transport across cellular membranes, transport reflects a balance between ion–water interactions (23) and ion–protein interactions (42). Water molecules and functional groups from proteins may interact directly with transiting ions (13, 18, 31, 32, 34), providing ligands and defining the local ion solvation structure.

An important factor in assessing whether channel and transporter proteins form binding sites that mimic the local hydration structures of permeant ions is the hydration properties of ions in the reference environment of bulk liquid water. Ions and water form preferred coordination structures, which may not be attainable in protein environments (28, 37, 43, 44).

Studies of ion hydration structure and hydration free energy benefit from the combination of experimental and theoretical approaches (26, 27, 45, 46). In the case of hydration structure, experiments can provide information about average water structure. Molecular simulations, verified against experimental data, can resolve average structure into contributions from individual water molecules. These contributions identify local hydration structure, the information sought here. The structural predictions can be scrutinized further by using local structures to build predictions of ion hydration free energies, also tested for consistency with experimental data in gas and liquid phases. In this way, local ion hydration structure can be reliably connected to ion hydration free energy, providing insights into the mechanism of ion hydration. This overall approach is described further in Section 4, below.

Quasi-chemical theory (QCT): theory that partitions free energy into three distinct contributions based on a clustering algorithm

Water: the reference environment for ion transport across cellular membranes

Neighborhood: neighborhood analyses describe the structures of the ligands closest to an ion and can reveal so-called split-shell coordination structures

1.1.1. Hydration structure. Experiments that probe ion hydration structure include neutron and X-ray diffraction techniques that report differential scattering cross sections leading to partial structure factors (27). An alternative technique, extended X-ray absorption fine-structure spectroscopy, also provides data related to partial structure factors (47–49). These factors can be determined with good accuracy and yield pairwise radial distribution functions (RDFs) between ions and water oxygen (O) molecules. The RDF establishes information that characterizes the structure of solvent around ions of interest. For example, integrating the RDF through an inner shell yields hydration numbers of ions.

In practice, significant challenges regarding good spectral resolution and momentum cutoffs (for diffraction research) are encountered in obtaining accurate experimental hydration numbers. Nevertheless, recent developments in both data acquisition and analysis, motivated in part by molecular simulation studies based on *ab initio* approaches and QCT (24), have significantly advanced experimental results (27). Even with accurate hydration numbers determined from experiments, information about local hydration structure may still be lacking. *Ab initio* molecular dynamics (AIMD) simulations can further differentiate local structural features, for example, disposition of the closest water molecule, from the aggregated hydration structure defined conventionally by RDFs.

As with experiments, AIMD simulation results are challenged by demands of realistic access to suitable ranges of space and time (50). Nevertheless, recent developments in both algorithms and computer power have led to improved information about ion hydration structures (51–59). Here, we highlight the correspondence between ion hydration structure illuminated by AIMD simulations and available experiments.

To resolve local structure, simulation calculations can provide natural neighborhood analyses of ion hydration structures, providing information not readily obtained from experiments. Those analyses distinguish water molecules directly contacting an ion from ligands that split time between ion contact and more distant solvent environments. Distinguishing non-split-shell and split-shell water molecules helps in assessing the hydration mimicry idea.

While they have not yet been broadly implemented (30, 46, 60–62), neighborhood analyses should be more widely used because of their clear conceptual connection to solvation free energy on the basis of molecular QCT. At the same time, solvation free energies computed by QCT test local structural predictions and facilitate the testing of concepts of solvation mechanisms based on coordination numbers and other primitive concepts described above for the design of biomimetic transport.

1.1.2. Hydration free energy. Predictions of ion hydration free energies from molecular simulations face numerous challenges. One significant challenge arises because ion–water interactions beyond the commonly used molecule–pair interaction models are complicated. These complications reflect solvent polarizability and multimolecule interactions generally, affecting interactions in the local solvation environment (63, 64). This complexity, again, calls for an approach that takes electronic degrees of freedom into account (50).

Another challenge arises with calculations of ion hydration free energies with QCT based on treating inner-shell clusters together with the initial assumption of small displacements (thus, harmonic motions) of water molecules neighboring an ion. Recent research has refined this issue, but it deserves further development (65).

Free energy contributions from hydration of isolated clusters are computed separately in QCT. Properties of these clusters are accessible from experiments, such as those using high-pressure mass spectrometry (66). Such experiments determine the free energies of equilibrium

cluster association reactions in the gas phase (67) and can also be compared directly with, or even incorporated into, QCT analyses.

Recent research (46, 65, 68) has provided examples of coupling between experiment and theory to predict ion hydration free energies, incorporating gas-phase ion clustering free energies into QCT for halide ions. These studies accounted for anharmonic vibrational motions observed spectroscopically in clusters with several coordinating water molecules (69). Furthermore, density functionals used in AIMD simulations were selected to reproduce peak positions in experimentally determined RDFs. Hydration free energy predictions yielded excellent agreement with the experimental hydration free energy of the neutral LiF pair. Importantly for our purposes, this research followed reliable identification of local hydration structure, which led to reliable ion hydration free energies. Details of the procedure, and applications to a variety of ions, are given below.

Specific ions:

an extended sequence of ions that show contrasting rejecting, permeating, and trapping behaviors in membrane transport

1.2. Ions in Protein Binding Sites

Ion channels and transporters are ubiquitous, and nature has evolved a variety of membrane proteins specialized to the transport of ions such as potassium (K^+), sodium (Na^+), calcium (Ca^{2+}), and magnesium (Mg^{2+}). The history of membrane transport proteins is now 7 decades old. Yet, new ion transport proteins, structures, functions, and mechanisms of both new and old transport proteins are discovered almost daily, making the field of ion channels and transporters one of the most active in molecular biology (15, 31, 32, 35–37, 42, 70–78).

Many ion channels catalyze rapid transport (10^6 – 10^8 ions/s) while simultaneously being highly selective for a specific ion. These two properties seem counterintuitive. Experimental results going back to pioneering research by Hodgkin & Keynes (79), however, indicate that ion channels that selectively catalyze rapid transport of ions have multiple sites where ions bind (15, 80). Models based on rate theory provide an intuitive explanation for the phenomenon of rapid transport facilitated by multiple binding sites (80, 81). A prerequisite, noted above (14), is that ion binding relative to aqueous solution should be weak for rapid transport.

As illustrated in **Figure 1**, the free energy wells and barriers for rapid translocation should be minimal and centered around the free energy for ion hydration in bulk water: $\mu_{M^{g+}}^{(ex)}(\mathbf{r}) \approx \mu_{M^{g+}}^{(ex)}$. Another ion may encounter large energetic barriers [$\mu_{M^{g+}}^{(ex)}(\mathbf{r}) \gg \mu_{M^{g+}}^{(ex)}$] and, therefore, be rejected. Alternatively, the channel pore may provide a more favorable environment compared with the bulk aqueous phase [$\mu_{M^{g+}}^{(ex)}(\mathbf{r}) \ll \mu_{M^{g+}}^{(ex)}$], trapping an ion by binding tightly and hence blocking the channel.

1.2.1. Ion properties. The hydration mimicry idea originated to explain separation between ions of the same charge but different sizes—specifically, for K channels that conduct larger K^+ preferentially over smaller Na^+ . Ions can also be distinguished by coordination number. Comparison between the coordination structure of K^+ in a binding site and that of K^+ in a neighboring water-filled cavity showed both ions with eightfold coordination (13). Earlier analyses of neutron scattering data also proposed eight as the preferred coordination number for K^+ in bulk liquid water (26, 82), although later research revised that number (26, 83–85). Altogether, these results supported the initial proposal of hydration mimicry as a mechanism for rapid and selective ion transport (12–15).

1.2.2. Ligand properties. Research outside the field of membrane transport proteins has led to a variety of ideas about which ligand properties underlie preferential solvation of specific ions, but the concepts do not always account for ion binding preferences demonstrated by protein binding

sites. One prominent concept points to ligand chemistry as a key factor in ion binding preferences (86); another identifies matching of ligand hydration free energy to ion hydration free energy (87). Recent tests of these concepts on ion binding to binding sites composed of acetate molecules found no support for the latter concept, called the equal affinities hypothesis (29). The same study reported support for the former concept, the ligand field strength hypothesis, but only when binding sites include the preferred number of ligands, as determined by free energy analysis. An important conclusion is that neither concept accounts for the role of the environment in binding site structure (29).

In proteins, the matrix surrounding binding sites, or properties of the binding sites themselves, may hinder ligand freedom to rearrange upon ion binding. Consequently, binding sites may form suboptimal arrangements for ion binding, leading to less-favorable ion binding (88).

Properties of a binding site that naturally take into account constraints from the environment include cavity size, or the distance between ion and ligand, and the number of ligands that coordinate bound ions. While hydration mimicry is the main idea to be tested here, cavity size was proposed as an initial explanation for the counterintuitive size discrimination of K channels, with a focus solely on well-fitting ion–ligand distances (89, 90). In both proposals, local ion solvation structure plays the key role in ion selection and, combined with the chemistry of the ligands, compensates for ion solvation requirements for rapid permeation (71).

These factors of ligand number and cavity size echo conclusions from earlier research on ion carriers such as the small molecule valinomycin. Although valinomycin lacks a transport pathway that would require a specific binding free energy consistent with permeation (**Figure 1**), it does bind larger K^+ selectively over smaller Na^+ ions (91). Notably, valinomycin binds K^+ using fewer ligands than K channels. Constraints on cavity size due to intramolecular bonds and the surrounding solvation environment provide a compelling explanation for selective K^+ binding by valinomycin (44). In view of experimental data that characterize K-channel binding sites as moderately inflexible when occupied by permeant ions, a constrained cavity size that provides a so-called snug fit to permeant ions might account for selective K^+ binding by K channels (92). A constrained cavity size, however, may inhibit transport of ions between well-fitting binding sites (28, 93).

1.3. Specific Ions and Proteins for Hydration Mimicry Analysis

Ions selected to test the hydration mimicry concept include both monovalent alkali metal ions [lithium (Li), Na, K, rubidium (Rb)] and divalent alkaline earth metal ions [Mg, Ca, strontium (Sr), barium (Ba)]. The protein binding sites analyzed here come from a celebrated bacterial K-selective channel (KcsA) (15), the recently discovered bacterial Mg-selective transporter (MgtE) (32, 33), and the voltage-gated bacterial Ca-selective channel (Ca_vAb) (34, 80).

In the results presented below, we report the size of the local solvation structures and the coordination numbers of the ions examined here. The most probable distances between ions and ligands, determined by the first maxima in RDFs and the distances reported in crystal structures, measure size. Cavity sizes should follow these quantities. The inner-shell radii, set by the first RDF maxima, set another measure of size. We discuss both of these size measures for ions in liquid water and compare them with ion–ligand distances in protein crystal structures for insights into hydration mimicry.

Comparisons of ion coordination properties include the number and chemistry of ligating atoms. Our main interest for testing the hydration mimicry idea is in the number of ligating atoms that directly interact with the ion in stable complexes. Additional considerations, to be highlighted in another publication, include the effect on ion solvation free energies from constraints on local binding site structures that may be imposed by the surrounding protein environment.

1.3.1. Specific ions. Among the monovalent ions, Na^+ and K^+ are well known for their roles in initiating and terminating action potentials (1). As analogs to K^+ and Na^+ , Rb^+ and Li^+ are also interesting monovalent ions. In laboratory settings, Li^+ ions show contrasting rejection behaviors, and Rb^+ ions permeate (31).

Among the divalent ions, Ca^{2+} and Mg^{2+} are common in biological systems. Homeostasis of these ions is tightly controlled by binding proteins, channels, exchangers, and pumps or transporters (95–97). Sr^{2+} and Ba^{2+} ions are not biologically relevant but are well-known blockers of K^+ permeation in K channels. These ions are used to understand the mechanism of K-channel function (17, 18, 20, 31, 98, 99). Despite their close similarity in size and identical +2 charge, Ba^{2+} and Sr^{2+} exhibit different blocking behaviors in K channels (100, 101). In particular, Ba^{2+} blocks bacterial K channels such as KcsA, but Sr^{2+} does not (19).

The comparison among ions presented here highlights patterns involving local solvation structure in water and channel binding sites among the eight ions selected for study. These ions span a range of sizes and charges. Ions of similar size include $\text{Li}^+/\text{Mg}^{2+}$ and $\text{Na}^+/\text{Ca}^{2+}$. Several ions treated here— Rb^+ , Ba^{2+} , and Sr^{2+} —resemble K^+ in size.

1.3.2. Specific channels and transporters. In K-selective channels such as the bacterial KcsA protein, crystal structures show dehydrated K^+ ions in four binding sites, numbered S1–S4 from the extracellular to the intracellular side (14). Structural studies also show dehydrated Ba^{2+} in the S4 binding site of bacterial K channels (17, 18, 20, 31). The environment varies around binding sites since water borders the ends of the selectivity filter (S1, S4) in the open state. Here, we consider an interior binding site (S2) that coordinates permeant ions with carbonyl O atoms from the protein backbone. We also consider the innermost binding site located near bulk liquid water (S4) and composed of the backbone and side-chain O atoms of four threonines (Thr).

Despite conservation of amino acid residues that form K-channel binding sites, the function of K channels can change under certain conditions. The bacterial KcsA channel catalyzes rapid passage of K^+ across membranes but rejects the smaller Na^+ ions by a high ratio of 1,000:1 in physiological conditions (1). By simply changing the solution environment from high to low K^+ concentration, the four conserved K^+ binding sites distort so that the channel switches from a conducting configuration to a nonconducting configuration (13). In the unusual absence of K^+ , Na^+ ions can also distort the channel structure and block ion permeation (14). In related NaK channels, two sites (S3 and S4) are identical to KcsA; nevertheless, both K^+ and Na^+ permeate equally well. Explanations of rapid, selective ion permeation in K channels should account for these intriguing observations, too.

The Ca_vAb crystal structure shows three distinct ion binding sites, with the middle one having the highest affinity. The presence of binding sites with different affinities is in good agreement with other experimental observations, and a so-called stairstep three-site rate theory model can explain both the high selectivity and transport rates observed for Ca_vAb channels (80). Here, we select the middle, highest-affinity Ca^{2+} binding site from Ca_vAb , which also rejects Mg (34).

The Mg-selective channels also contain three primary ion binding sites. While both Mg^{2+} and Ca^{2+} ions can bind to the M1 binding site, the M3 binding site selectively binds Mg^{2+} ions (33). For testing the hydration mimicry idea, we select the Mg^{2+} -selective M3 binding site from MgtE.

For the applications discussed here, the free energy for ion binding to a channel protein, relative to its hydration free energy, is central to understanding the thermodynamic driving forces and mechanisms of ion permeation. Our tool is QCT, discussed further below. QCT is a statistical mechanical theory based on close solution contacts treated at chemical resolution by ab initio methods (25, 102, 103). The exploitation of chemical calculations is key to resolving ion specificity

Surface potential:
does not affect
predictions of
differences between
ions of the same
charge

in these problems. The coupling of structure with thermodynamics aids in understanding the molecular mechanisms.

In the remainder of this review, we first discuss basic aspects of QCT, including surface potentials relevant to ion hydration calculations involving interfaces, and application of QCT to protein binding sites. We then survey our broad set of simulation results on hydration structures for relevant metal ions in water. Next, we present our results on ion hydration free energies, obtained by analyzing local hydration structures in the QCT formulation. Finally, we compare local ion hydration structures in liquid water with local ion solvation structures in protein binding sites as a structural test of the hydration mimicry concept. We reserve for future research the comparison of ion solvation free energies in channel binding sites to ion hydration free energies. That comparison will take into account the environment surrounding the binding sites, including the possibility that the environment constrains local binding site structure (28, 88, 103).

2. QUASI-CHEMICAL THEORY

QCT was developed (25, 102, 103) for exactly the problems considered here: interaction free energies of specific ions in solutions and protein binding sites (29, 61, 102–107). The excess chemical potential

$$\mu_{M^{q+}}^{(\text{ex})} = \mu_{M^{q+}} - kT \ln (\rho_{M^{q+}} \Lambda_{M^{q+}}^3) \quad 1.$$

is obtained from the full chemical potential less the ideal contribution indicated. Here, k is the Boltzmann constant, T is the temperature, $\rho_{M^{q+}}$ is the number density of the ion of interest, and $\Lambda_{M^{q+}}$ is the thermal de Broglie wavelength (108) of species $M^{q+}(\text{aq})$. This interaction free energy analysis can also provide

$$\mu_{M^{q+}}^{(\text{ex})}(\mathbf{r}) = \mu_{M^{q+}} - kT \ln (\rho_M(\mathbf{r}) \Lambda_{M^{q+}}^3), \quad 2.$$

describing binding at locations \mathbf{r} , generally (108).

2.1. Inner-Shell Clusters

The physical concepts underlying QCT develop from consideration of association equilibria:



The populations of the clusters $(\text{H}_2\text{O})_n M^{q+}$ are identified by a clustering algorithm, according to which proximal ligands of a specific M^{q+} are defined as inner-shell partners of that ion. The theory develops by treating the cluster $(\text{H}_2\text{O})_n M^{q+}$ as a molecular component of the system.

QCT is, then, a fully elaborated statistical mechanical theory that enables modern molecular computation (25, 102, 103). Moreover, QCT can be closely coordinated with molecular simulation calculations, thereby providing a compelling molecular theory of liquid water itself (109).

Thus, application of QCT begins with identification of the inner-shell configurations of an ion of interest. A simple procedure is to identify those water molecules with O atoms within a distance λ from a metal ion as inner-shell partners. From there, with n water ligands in the cluster, the free energy is elaborated as

$$\mu_{M^{q+}}^{(\text{ex})} = -kT \ln (K_n^{(0)} \rho_{\text{H}_2\text{O}}^n) + kT \ln p_{M^{q+}}(n) + \left[\mu_{(\text{H}_2\text{O})_n M^{q+}}^{(\text{ex})} - n\mu_{\text{H}_2\text{O}}^{(\text{ex})} \right], \quad 4.$$

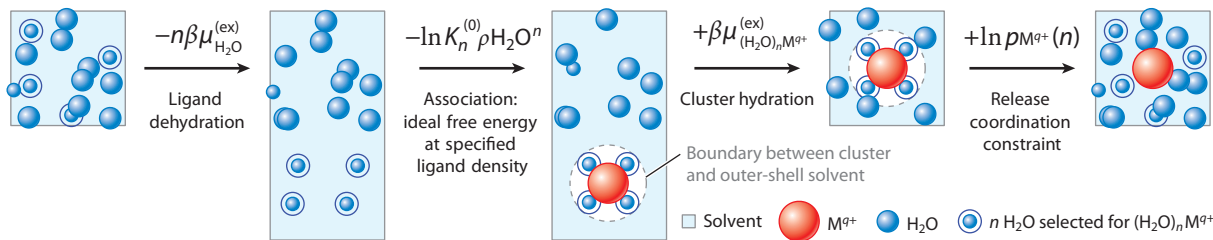


Figure 2

Hydration free energy of solute M^{q+} (red sphere), interpreted on the basis of Equation 4. The central feature of the quasi-chemical theory approach is analysis of the cluster $(\text{H}_2\text{O})_nM^{q+}$. Clusters of an ion and a selection of n inner-shell waters (blue spheres inside circles) associate in an ideal gas phase. Cluster solvation and water desolvation occur from the aqueous phase. Dashed circles indicate the boundary between the cluster and the aqueous phase. Figure adapted from Reference 94.

without statistical mechanical approximation. This formula is correct for any physical choice of λ and n . **Figure 2** guides us through the terms of Equation 4, which we discuss below.

The clustering free energy for Equation 3 is based on the equilibrium ratio

$$K_n = \frac{p_{M^{q+}}(n)}{p_{M^{q+}}(0)\rho_{\text{H}_2\text{O}}^n}. \quad 5.$$

The factor $K_n^{(0)}$ is the equilibrium constant K_n evaluated for the case where the external medium is an ideal gas. Evaluation of $K_n^{(0)}$ is accessible with widely available tools of molecular computational chemistry and can be validated against high-pressure mass spectrometry data (66, 67, 110–114).

The ideal gas characteristic $K_n^{(0)}$ conventionally takes $p = 1$ atm, thus identifying the ideal density p/RT with $p = 1$ atm. Our applications target $\rho_{\text{H}_2\text{O}} = 1$ gm/cm³ as the density of liquid water at $T = 298$ K and $p = 1$ atm. Then, $\rho_{\text{H}_2\text{O}}RT \approx 1,354$ atm. These density factors describe the availability of water for binding the ion. In the application to ion hydration, this availability is enhanced by a factor of 1,354 relative to the ideal $p = 1$ atm value.

Practical calculations of the outer-shell free energy term $[\mu_{(\text{H}_2\text{O})_nM^{q+}}^{(\text{ex})} - n\mu_{\text{H}_2\text{O}}^{(\text{ex})}]$ are set by adopting a statistical thermodynamic model of the environment of the $(\text{H}_2\text{O})_nM^{q+}$ cluster for the incipient free energy balance of Equation 4. Here, we employ the polarizable continuum model (PCM) (115). With PCM, the external boundary of the cluster solute is defined by spheres centered on each of the atoms. PCM results are sensitive to the values of the radii, but sensitivity to the values of the radii often balances out in the free energy difference when the ion is buried by the ligands.

Finally, **Figure 2** identifies the contribution $kT \ln p_M(n)$ with release of the constraint requiring n waters in ion association. The left side of Equation 4 is independent of n , so the complement provides $kT \ln p_M(n)$ to within a constant. Considering a specific λ , the minimum value of $kT \ln p_M(n)$ identifies the most probable n , which we denote by \bar{n} . Then we drop that statistical contribution:

$$\mu_{M^{q+}}^{(\text{ex})} \approx -kT \ln \left(K_{\bar{n}}^{(0)} \rho_{\text{H}_2\text{O}}^{\bar{n}} \right) + \left[\mu_{(\text{H}_2\text{O})_{\bar{n}}M^{q+}}^{(\text{ex})} - \bar{n}\mu_{\text{H}_2\text{O}}^{(\text{ex})} \right]. \quad 6.$$

Although \bar{n} minimizes that approximation error, the magnitude of the correction can be estimated from simulation results.

The advantage of QCT is that it separates solvation free energies into components from inner-shell and outer-shell solvent molecules, addressing the chemical physics issues in analysis of clusters. These issues include proper overlap repulsions, polarizability, charge transfer, London

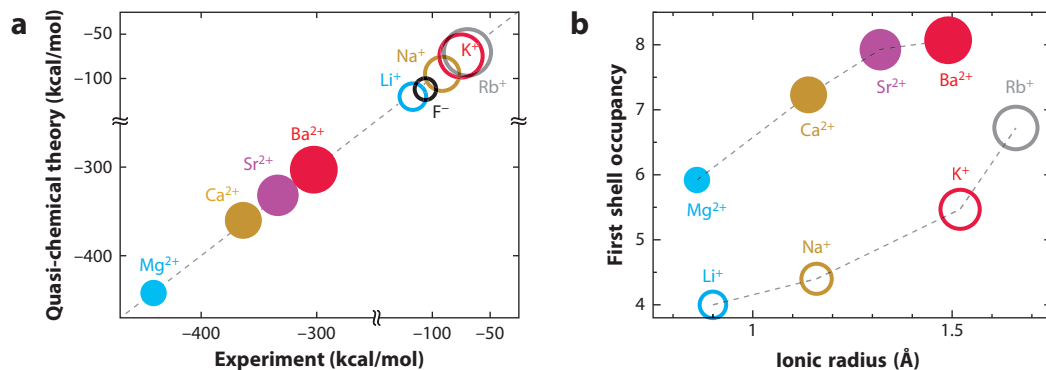


Figure 3

(a) Comparison between hydration free energies calculated from quasi-chemical theory (QCT) and the experimental tabulation of Reference 130, except for the F^- value, which was updated in Reference 132. Note that internal consistency of free energies for each collection of identically charged ions supports the view that any surface potential is treated reasonably. (b) Occupancy of the nearest hydration shell defined by the minima in radial distribution function (Figure 4) as a function of ionic radius. Water occupancy increases with increasing ion size, and more water molecules occupy the first shell of divalent (filled circles) than monovalent (open circles) ions. Colors match for ions of the same size.

dispersion interactions, n -body ligand interactions generally, distortion of flexible ligands, and zero-point motion of the cluster.

Water occupancy:

What are the probable $Ba(H_2O)_m$ $(Thr)_{n-1}^{2+}$ coordination cases for given Thr solution concentrations?

2.2. Potential of the Phase

Discussion of surface potentials highlights the subtlety of experimental testing of computed single-ion free energies (Figure 3). To that end, we augment the free energies of Equation 2 according to

$$\mu_{M^{q+}} = qe\Phi + kT \ln(\rho_{M^{q+}} \Lambda_{M^{q+}}^3) + \mu_{M^{q+}}^{(ex)} \quad 7.$$

by the electrostatic contribution, $qe\Phi$, for each of the conducting phases considered (116). Since Φ does not depend on chemical details of the ion, this extension plays no role in assessing the free energy of neutral combinations of ions. Φ depends neither on the ion size or structure nor on the distribution of electric charge within the ion. We refer to Φ as the potential of the phase. This quantity is determined through Poisson's equation of electrostatics, with charge densities for the generally heterogeneous system and boundary conditions. Φ thus depends on conditions bounding and external to the phase. Considering a conducting homogeneous fluid phase, Φ is a constant throughout (117). The bulk composition is charge neutral for such a phase.

For the case of two conducting fluid phases in equilibrium with respect to ion transfer between the phases, the difference $\Delta\Phi$ —the contact or junction potential (118)—can be tied to conditions of transfer equilibrium of ions and the neutrality of the bulk compositions (118–121). For a q - q electrolyte MX,

$$2qe\Delta\Phi = -\Delta \left[\mu_{M^{q+}}^{(ex)} - \mu_{X^{q-}}^{(ex)} \right]. \quad 8.$$

The right-side characteristics need not address the interface between the two phases but rather are aspects of the bulk solutions for the case $\Phi = 0$ —or some other fiducial value—for each phase considered individually, as is clearly permissible.

Although the spatial transition of Φ through an interfacial region from one homogeneous conducting solution to the other is more complicated, the simple result in Equation 8 was emphasized many years ago (118–121): “[F]or the junction potential the ideal solution limits differ in general from the pure-solvent values” (118, p. 3836). Furthermore, “since all real polar solvents are to some extent ionized, one has to take this effect into account in relating theory to experiments” (118, p. 3838). This situation does not seem to be widely appreciated.

There is broad interest in the idealized case of the fluid electrolyte solution bounded by a dielectric (nonconductor), perhaps a vacuum. This is the context for discussion of a surface potential (122). The solution, being a conductor, will still exhibit a spatially constant Φ , but the electrostatic potential will vary through regions bounding and exterior to the solution. The change in the electrostatic potential with passage out of the solution then requires further specification. Further theoretical modeling specification is simpler if a submacroscopic cavity is imposed internally. Then, the contacts of the solution with the cavity can be studied (123, 124). Remaining questions include whether changes in the electrostatic potential are satisfactorily independent of cavity size and whether the electrostatic potential might be spatially constant enough to serve in the thermodynamic formulation (Equation 7) for ions with different distributions of charge.

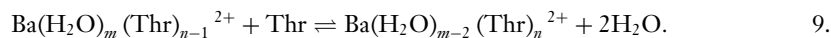
Reserving such issues for future research (125), we now discuss the relevance of the QCT approach, based on Equation 6. Since Equation 3 is balanced with respect to charge, the K_n of Equation 5 do not involve the potential of the phase (108). The examination of the TATB (tetraphenyl-arsonium/tetraphenyl-borate) hypothesis (55, 124, 126–129), and Marcus’s (126, 130) modeling of his tabulated values to depend quadratically on ion charge, makes these values natural for comparison with the QCT single-ion free energies that use the PCM for the cluster free energy of Equation 6. That the values of an alternative tabulation (131) are distinctly different is a cautionary point.

2.3. Quasi-Chemical Theory and Protein Binding Sites

Of special interest are the ion free energies $\mu_{M^{y+}}^{(ex)}(\mathbf{r})$ at a defined binding site (Equation 2) (**Figure 1**). QCT, being a general approach, is applicable to those problems (28–30, 64), though QCT deserves further development and detailed refinement for that context.

Here we exemplify one approach by using the context of Ba^{2+} occupying the innermost binding site of the K channel (S4). We begin with the K-channel crystal structure (Protein Data Bank accession number 1K4C) and the S4 site occupied by Ba^{2+} . Four Thr amino acids interact with Ba^{2+} in a bidentate fashion. Therefore, we build $\text{Ba}(\text{Thr})_4^{2+}$ clusters; an energy-optimized cluster structure shows that all Thr O atoms are displaced less than 1 Å from the crystal structure for the occupied binding site. This result is consistent with a physical intuition underlying QCT, namely that interactions of metal ions with near neighbors are localized, hugely stabilizing, and of utmost importance (45, 62, 102).

QCT addresses the solvation free energy of Ba^{2+} on the basis of analysis of clusters that may form:



Note that Equation 9 makes the reasonable assumption that two H_2O molecules naturally replace one Thr ligand. The equilibria ($n = 1, \dots, 4$) describe the formation of a binding site encapsulating a Ba^{2+} ion. From the initial ($n = 1$) state to the final ($n = 4$) state, this process converts hydrated Ba^{2+} ions to Ba^{2+} ions centering a model binding site. The free energy change for this process depends on the concentrations of the species involved; that is, a full description requires

Split-shell coordination:

the sixth nearest neighbor of $K^+(aq)$ sometimes occupies an innermost shell and, at other times, outer hydration shells

considering a standard state. We note above with Equations 4 and 5 that QCT properly resolves a standard state.

The equilibria (Equation 9) can organize a solution chemistry experiment involving an aqueous solution of a Ba^{2+} electrolyte as a medium for dissolution of Thr. The dissolved concentration of Thr would be tracked, and the coordination of Ba^{2+} by the Thr would be interrogated. The question, “What are the probable $Ba(H_2O)_m(Thr)_{n-1}^{2+}$ coordination cases for given Thr solution concentrations?” would naturally arise. Alternatively expressed: From the Thr completion side of the scheme (Equation 9), how much would the H_2O activity have to increase, by dilution of the Thr, for H_2O molecules to disrupt the $(Thr)_4$ binding site? Although this solution chemistry experiment would be an exceedingly natural assessment of biomolecular hydration mimicry, as far as we know it has not been done. Answers to such questions, and the natural follow-up questions, would address current issues of H_2O occupancy of K channels (37, 78, 133, 134).

3. ION HYDRATION STRUCTURE

Characterization of local ion hydration structure provides data essential for evaluation of the hydration mimicry concept. RDFs (Figure 4) of O (water) obtained from AIMD simulations for eight metal ions in water define inner-shell structures for alkali metal ions and alkaline earth metal ions. These AIMD results are consistent with accurate experimental determinations of peak positions (Table 1) and with other studies of particular cases (135–137). These ions are often compared in order to investigate effects of the ion charges and sizes on channel behavior. For smaller ions, there is an obvious separation between inner and outer hydration shells. As the ion size increases from Li^+ to Rb^+ and from Mg^{2+} to Ba^{2+} (Figure 4), the mean inner-shell occupancies become less distinct.

Neighborhood decompositions (138, 139) of those distributions characterize the natural hydration shell structure (28, 62). For the monovalent ions considered, the nearest four water molecules suffice to describe the RDF maxima, even though the total occupancy of the inner shell increases with ion size (Figure 3). Six water molecules suffice for the RDF maxima for the alkaline earth ions, but the inner-shell occupancies reach six or eight (8).

Note that sometimes a neighbor distribution can be multimodal; see, for example, the case of $n = 6$ for $K^+(aq)$ (Figure 4). We call these split-shell cases. Since the basic development (Equation 4) is correct independently of λ and n , we could agree to limit QCT applications to non-split-shell cases of λ and n , or we could implement more-involved computational research to treat the multimodal occupancies directly (65).

While hydration properties of the monovalent ions have been studied extensively, fewer studies have reported on the hydration properties of divalent ions. Mg^{2+} hydration has long been of biophysical interest. Dudev et al. (140) used electronic structure calculations to evaluate energy changes associated with replacing water molecules with other ligands. Six water molecules established the nominal coordination number for the $Mg^{2+}(aq)$ ion (107). Such results are consistent with X-ray diffraction measurements in an $MgCl_2$ solution (141) and our AIMD results (Figure 4).

Our RDF for the Ca^{2+} ion, and its neighborhood decomposition (Figure 4), suggests that the eighth water molecule splits occupancy between the inner and outer hydration shells, giving a hydration number between seven and eight. In contrast, Marcus (130) and Dudev & Lim (107) predicted a hydration number of seven for $Ca^{2+}(aq)$. That possibility deserves further investigation.

Previous AIMD simulations (142, 143) calculated a mean inner-shell occupancy of 7.5 for $Sr^{2+}(aq)$, lower than the values of 9.3 and 14.9 (144) from experimental data. Our result (7.9) supports the previous simulation effort. Although simulation and experiment differ in this respect,

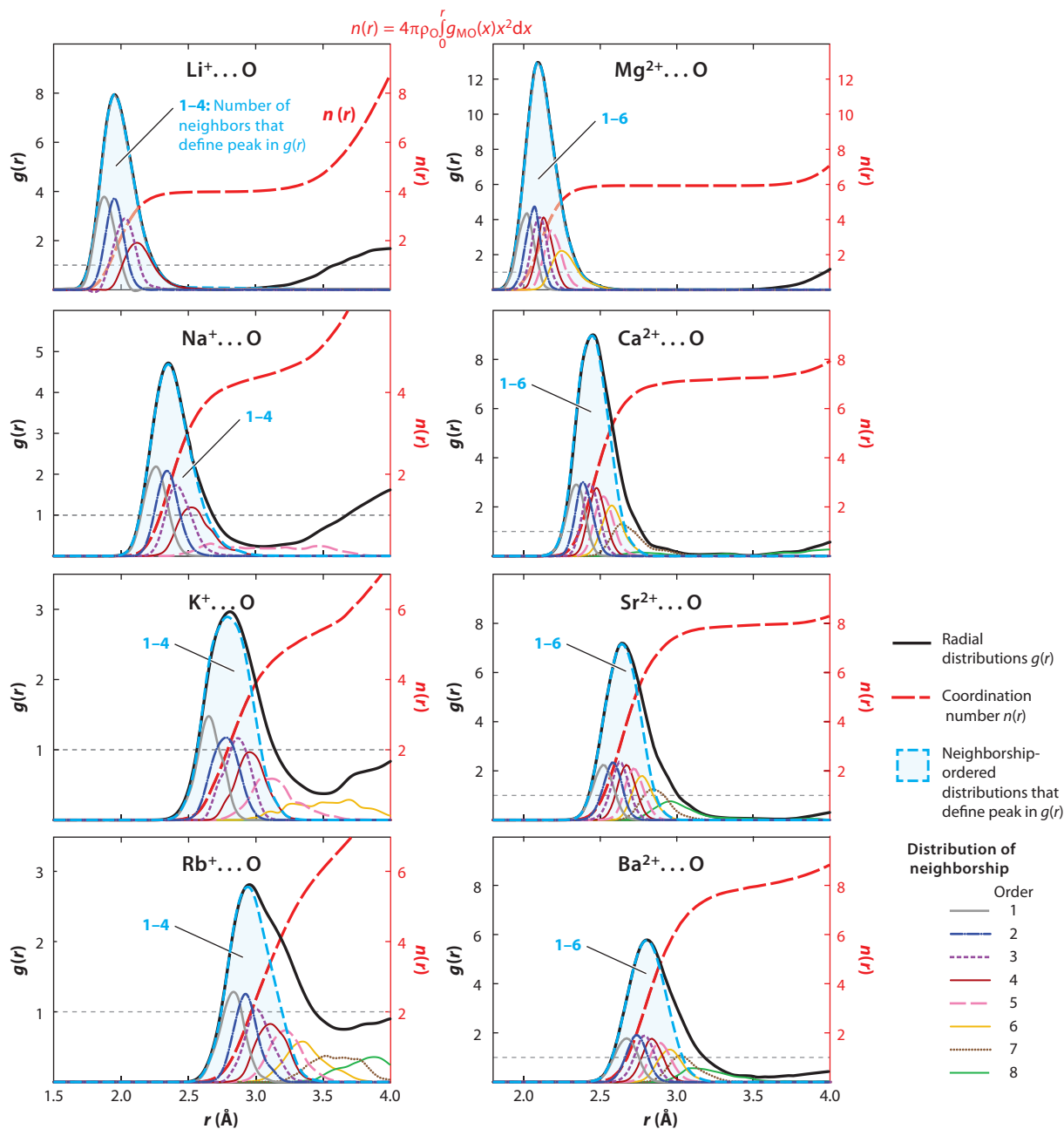


Figure 4

Radial distributions [$g(r)$; thick black lines] of water O atoms around eight metal ions, together with their decomposition into neighborhood-ordered distributions (thin, multicolored lines; 138, 139). Coordination numbers [$n(r)$; thick red dashed lines, right y axis] are obtained by integrating under $g(r)$ curves. Neighborhood-ordered distributions that denote the peaks in $g(r)$ (blue dashed lines) are indicated by number (blue). Data come from ab initio molecular dynamics simulations (references in **Table 1**). Peak positions agree well with experiments (**Table 1**).

Table 1 Comparison of radial positions of the RDF maxima observed in AIMD simulations

Ion	AIMD	Exp.	Ion	AIMD	Exp.
Li ⁺	1.95 (129, 146)	1.96 (27)	Mg ²⁺	2.09 (62)	2.04 (147)
Na ⁺	2.37 (26)	2.38 (48)	Ca ²⁺	2.45 (62)	2.43 (147, 148)
K ⁺	2.73 (26, 28)	2.73 (49)	Sr ²⁺	2.64 (30)	2.63 (149, 150)
Rb ⁺	2.95 (45)	3.10 (151)	Ba ²⁺	2.81 (61)	2.80 (152)

Units are in angstroms. References are in parentheses.

Abbreviations: AIMD, ab initio molecular dynamics; Exp., experimental value; RDF, radial distribution function.

our RDF peak positions closely match the experimental results (**Table 1**), and predictions of hydration free energy match experimental values (**Figure 3**), suggesting a reliable hydration number prediction.

An octa-coordinated hydration structure for Ba²⁺(aq) was proposed in 1933 (145). Although several studies have interceded since, our result lends support to that proposal and experimental data (**Table 1**). The hydration free energy computed on this basis matches experimental results (**Figure 3**), as presented below.

4. ION HYDRATION FREE ENERGY

Ion hydration free energies set a reference value for ion permeation through protein channels and transporters. Comparisons of hydration free energies with experimental results provide baseline tests of molecular statistical thermodynamic theory. For ions, these comparisons raise the issue that hydration free energies are obtained by manipulation of neutral material combinations. Thus, tabulated single-ion free energies, used here, incorporate extrathermodynamic assumptions and disagree somewhat when different assumptions are used (130, 131). We respond to this issue partially here, in two different ways.

Our first partial response is that computed theoretical free energies can be tested with results for neutral combinations of ions. Doing so requires application of the theory to an example anion (46, 65, 68) in addition to the monoatomic metal ions of primary interest here. To the extent that the theory performs satisfactorily for the neutral test case, comparisons among different cations are also supported. **Figure 3** presents such an initial comparison, supported by a QCT calculation for F⁻(aq) (46, 68). Combining results for LiF produces -227.5 kcal/mol (QCT), in fair agreement with experimental tabulations, which range between -229 and -232 kcal/mol (67, 130, 131). This discussion is only a partial response for molecular theory because it does not account for the advantages from dissection of a net result into physically meaningful parts, the single-ion free energies.

Our second partial response is that the theory should address the problem sufficiently thoroughly that the accuracy of the individual steps of the theory can be checked. Developing this second partial response provides the opportunity to investigate the components that are central to the performance of QCT theory.

Considering the several components that are combined to evaluate the net free energy, we base the following discussion on the examples of Rb⁺ and Ca²⁺ (**Figure 5**). These free energy contributions (**Figure 5**) are all substantial on a chemical energy scale, that is, comparable to traditional chemical bond energies.

In light of the trends in each free energy contribution (**Figure 5**), the gas-phase association term becomes more favorable with increased n for Rb⁺ and Ca²⁺. The contribution to hydration free energy from water molecules beyond the inner-shell clusters becomes less favorable as cluster

Chemical energy scale: set by traditional chemical bond energies and appropriate for ion hydration free energy

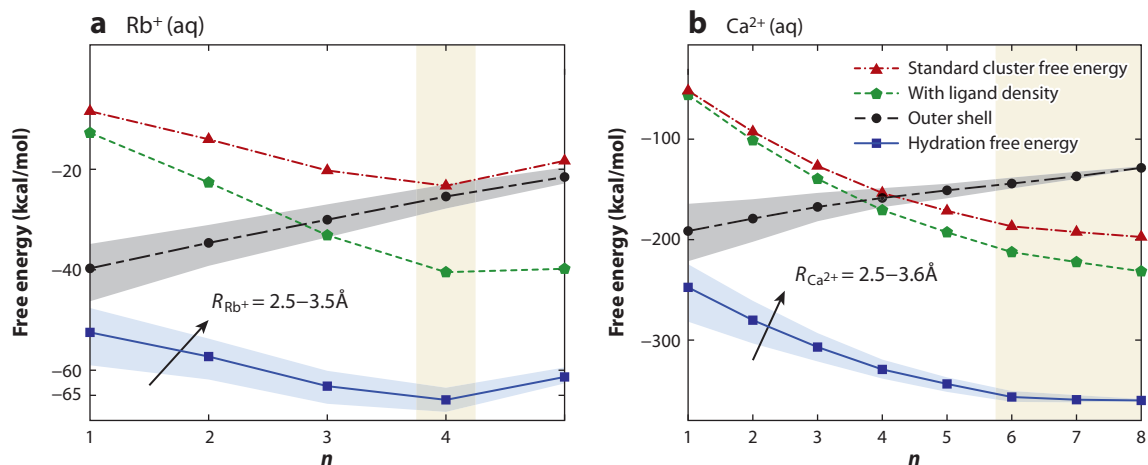


Figure 5

Dependence of individual quasi-chemical theory (QCT) contributions on inner-shell occupancy, n , for (a) $\text{Rb}^+(\text{aq})$ and (b) $\text{Ca}^{2+}(\text{aq})$. Tracking $-kT \ln p(n)$, the net QCT combination is minimal for the most probable coordination number (**Figure 4**). For probable occupancies (yellow shading), the net result (blue shading spanned by arrow) is insensitive to R_{M^q} used to calculate the outer-shell contribution (gray shading) and closely agrees with the experimental tabulation of Reference 130. The standard cluster free energy contribution at the proper ligand density (green pentagons) accounts for more than half of the hydration free energy.

sizes increase. This outer-shell contribution also varies with boundaries, explored here for λ set between the first maximum and minimum of the RDF for each ion. The variation with boundary becomes small upon reaching clusters with full occupancy of the inner shell, at $n = 4$ for Rb^+ and $n = 6-8$ for Ca^{2+} .

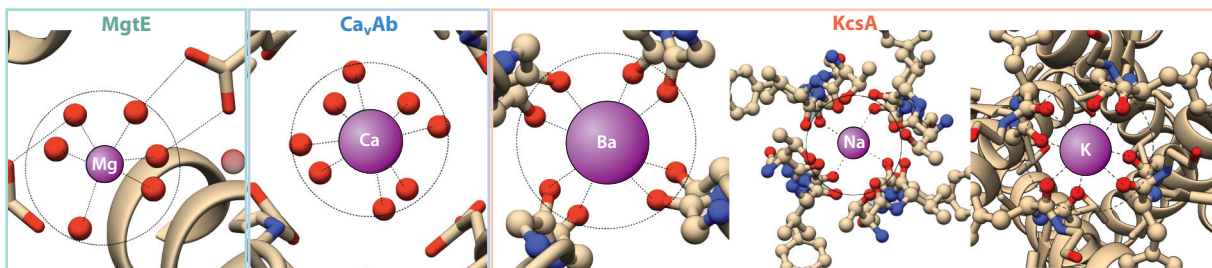
The variation of the free energy results of **Figure 5** with λ and n is encouragingly simple. Nevertheless, the dielectric model for the outer-shell contributions, here PCM, can be problematic when n differs substantially from full occupancy (45). In contrast, the free energies can be satisfactory when this inner-shell occupancy is saturated because of the balance between the cluster and ligand terms of the rightmost contribution in Equation 6. Sensitivity to adjustment of boundaries for dielectric models is then moderated because the adjusted boundaries are somewhat buried in the cluster, although otherwise balanced. This point is significant because continuum models are typically sensitive to the boundaries, which are not independently defined by physical principles. Indeed, boundaries (153, p. 784) are “a complicated function of density, temperature, and molecular parameters.” Nevertheless, the rightmost (cluster) contribution of Equation 6 is the principal theoretical approximation in QCT calculations.

5. LOCAL STRUCTURE COMPARISON

We can compare hydration structures with crystallographic data for ions in the binding sites of proteins. This structure comparison takes us another step forward in testing the hydration mimicry concept.

We begin with proteins permeable to Mg^{2+} and Ca^{2+} . Crystallographic data are available for recently discovered Mg transporter structures (32, 33, 107). Compare the Mg^{2+} ion in the Mg transporter binding site (**Figure 6**) (33) with a PCM-optimized structure of $[\text{Mg}(\text{H}_2\text{O})]_{6+1}^{2+}$, composed of six water molecules occupying the inner solvation shell and one water molecule in the second shell. In bulk solution (**Figure 4**), six inner-shell water molecules establish the

a X-ray crystal structures of membrane transport proteins



b Solution-optimized ion–water clusters

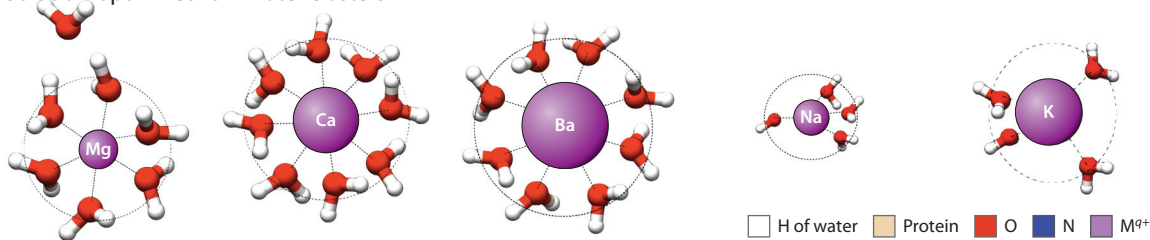


Figure 6

(a) X-ray crystal structures of ions (M^{q+}) and water molecules (*isolated red spheres*) inside membrane transport proteins MgtE [Protein Data Bank accession number 4U9L (33)], Ca_vAb [4MS2 (34)], and KcsA [1K4C (13)], with (b) solution-optimized ion–water clusters. Except for the K^+ case (*far right*), the ion coordination inside each protein mimics the near-neighbor hydration structure, consistent with the hydration mimicry idea.

near-neighbor distance of 2.1 Å. Unlike K channels, where K^+ ions directly contact protein O atoms, Mg^{2+} carries along its aqueous inner shell as it occupies the protein binding site.

Similarly, the Ca_vAb structure shows a fully hydrated Ca^{2+} ion coordinated by eight water molecules (34), which further coordinate with aspartate and asparagine side-chain O atoms of the channel in the outer solvation environment. In aqueous solution, six water molecules establish the near-neighbor distance at 2.5 Å, although up to eight can be considered in broader settings (Figure 5).

Thus, the divalent ions observed in the crystal structures of Ca^{2+} and Mg^{2+} selective binding sites bind directly with local water molecules (Figure 6) (154). This hydration mimicry is nearly perfect, and longer-ranged effects come to the foreground with further selectivity.

In the K-selective KcsA channel, K^+ ions can occupy each of the four binding sites (S1–S4) in the selectivity filter, coordinated by eight O atoms from carbonyl groups either from the protein backbone or from Thr side chains (Figure 6) (14). The average distance between the O atoms and K^+ , the cavity size, is 2.8 Å. No water molecules contact K^+ in this case.

In comparison, AIMD studies of K^+ hydration structure show occupancy in the inner shell by four to six water molecules (Figure 4). The peak in the RDF saturates with four water molecules, located 2.7 Å from the ion, although six can be considered in broader settings (Figure 5). The sixth water molecule splits occupancy between inner and outer shells. In contrast to the eight ligating O atoms in the KcsA crystal structure, in bulk solution the eighth water molecule occupies the outer solvation volume.

The differences in K^+ contacts raise several questions. First, why is the number of K^+ inner-shell O atoms lower in water than in the KcsA binding site? Second, how can moderate transfer

free energy profiles (**Figure 1**) arise when local structures differ? Third, can local contacts account for selective binding of K^+ over Na^+ ? Prior studies have addressed these questions (28, 88), and we expect they will be reviewed further in upcoming research.

Since K-selective KcsA channels select against Na^+ ions by a factor of 1,000:1, the rejected ions seldom competitively occupy the KcsA pore. But in the absence of K^+ , Na^+ binds to a site between the K^+ binding sites (16). The Na^+ ions bind between sites S3 and S4, coordinated by four carbonyl O atoms arranged in a planar geometry and separated from the ion by 2.4 Å.

AIMD studies indeed show Na^+ hydrated by four to five water molecules (**Figure 4**). The fifth water molecule splits occupancy between inner and outer shells. Thus, when a Na^+ ion enters a K-selective channel, it binds in a configuration that mimics the bulk hydration structure. In this case, however, that binding leads to a trapped ion that blocks permeation. For the well-known K-channel blockers Sr^{2+} and Ba^{2+} , solution hydration structures appear similar, as expected for ions of identical charge and similar size. Six water molecules saturate the principal maxima of the RDFs, although up to eight might be considered in broad settings.

Structural data for Ba^{2+} in K channels were recently published (18), but similar data for the Sr^{2+} ion are unavailable. In this Ba^{2+} crystal structure, eight O atoms from the innermost (S4) K-channel selectivity filter constitute the binding contacts (**Figure 6**). With an inner-shell occupancy of eight and a cavity radius of 2.8 Å, the protein nicely mimics the hydration environment of Ba^{2+} . Structural similarity thus supports the hydration mimicry idea, but evidently the Ba^{2+} ion is too stably bound (**Figure 1**).

To summarize these local structural comparisons, hydration mimicry appears applicable to all ions considered here, except for K^+ in the K channels that inspired the concept. In that case, two more O atoms contact K^+ in channel binding sites than in aqueous solution. In all other cases for which crystal structures are available, local solvation structures in crystallized channel binding sites arrange to fit each ion with contact distances and numbers anticipated from accurate solution information. In some cases, hydration mimicry leads to rapid ion permeation, but in other cases, mimicry leads to trapped ions and blocking of permeation.

6. CONCLUSIONS

The concept of hydration mimicry has long been applied to the functional design of membrane ion channels (15). This concept enters with coarse descriptors of ions and their interactions—that is, sizes of protein binding sites and of ions, of the dielectric response of the environment, and of the ion binding free energies described with these coarse factors. The research described here builds a rigorous foundation for several of these factors, including ion sizes and hydration structures (**Figures 3** and **4**). We emphasize that these primitive data, specifically the neighborhood analyses depicted in **Figure 4**, were not assured at the initiation of this research (24–27).

Ion free energies (**Figure 1**) are natural assessments of these primitive descriptors, and QCT (25) addresses these free energies (**Figure 3**), as it was designed to do (**Figure 5**). This theory provides a comprehensive description of the relative stability of the end points of the ion transfer process. It also allows isolation of inner-shell (chemical contacts) and outer-shell interactions to illuminate mechanistic aspects of ion transfer. This information can be useful for designing membranes for specific phase-transfer processes (7, 11).

For the membrane transport proteins assessed here, hydration mimicry applies in most, but not all, cases. It applies to ions that permeate rapidly, as well as ions that block permeation. Nevertheless, the dynamics of the ion transfer process may also depend on the atomic-scale dynamical flexibility of the thermal systems considered (102).

Cavity radius of ion: boundary for dielectric continuum model that is less important for clusters with full occupancy of the inner shell

SUMMARY POINTS

1. Properties that differentiate ions include size, charge, and coordination number.
2. Neighborhood analyses describe the structure of the n closest ligands to an ion, define direct contacts, and reveal split-shell coordination (defined in Sections 1.1.1 and 3).
3. Direct-contact structure determinations and QCT work together to unravel the mechanisms of ion binding.
4. Interactions of metal ions with near neighbors are as strong as chemical interactions, but selectivity of ion transport depends on the balance of ion coordination equilibria, including the aqueous solution end points of the transport.
5. The hydration mimicry concept applies to ions that permeate rapidly and to ions that block permeation; thus, hydration mimicry does not necessarily guarantee rapid ion permeation.

FUTURE ISSUES

1. The stability of protein binding sites should be characterized by manipulation of water activity. What are the probable $\text{Ba}(\text{H}_2\text{O})_m(\text{Thr})_{n-1}^{2+}$ coordination cases for given Thr solution concentrations?
2. For the paradigmatic KcsA channel, are structural differences between K^+ binding in the selectivity filter and that in bulk water a key to K^+/Na^+ selectivity?

DISCLOSURE STATEMENT

The authors are not aware of any affiliations, memberships, funding, or financial holdings that might be perceived as affecting the objectivity of this review.

ACKNOWLEDGMENTS

We thank Thomas L. Beck for helpful discussions. Sandia National Laboratories is a multimission laboratory managed and operated by National Technology and Engineering Solutions of Sandia, LLC, a wholly owned subsidiary of Honeywell International, Inc., for the US Department of Energy's National Nuclear Security Administration under contract DE-NA-0003525. The writing of this review was supported by Sandia's Laboratory Directed Research and Development program and performed, in part, at the Center for Integrated Nanotechnologies. This review describes objective technical results and analysis. Any subjective views or opinions that might be expressed in this review do not necessarily represent the views of the US Department of Energy or the US Government.

LITERATURE CITED

1. Hille B. 2001. *Ionic Channels of Excitable Membranes*. Sunderland, MA: Sinauer. 3rd ed.
2. Wulff H, Zhorov BS. 2008. K^+ channel modulators for the treatment of neurological disorders and autoimmune diseases. *Chem. Rev.* 108:1744–73

3. Zhao Y, Huang J, Yuan X, Peng B, Liu W, et al. 2015. Toxins targeting the K_v1.3 channel: potential immunomodulators for autoimmune diseases. *Toxins* 7:1749–64
4. Pardo LA, Stühmer W. 2014. The roles of K⁺ channels in cancer. *Nat. Rev. Cancer* 14:39–48
5. Banerjee A, Lee A, Campbell E, MacKinnon R. 2013. Structure of a pore-blocking toxin in complex with a eukaryotic voltage-dependent K⁺ channel. *eLife* 2:e00594
6. Morales-Lázaro SL, Hernández-García E, Serrano-Flores B, Rosenbaum T. 2015. Organic toxins as tools to understand ion channel mechanisms and structure. *Curr. Top. Med. Chem.* 15:581–603
7. Cygan R, Brinker C, Nyman M, Leung K, Rempe SB. 2008. A molecular basis for advanced materials in water treatment. *MRS Bull.* 33:42–47
8. Park HB, Kamcev J, Robeson LM, Elimelech M, Freeman BD. 2017. Maximizing the right stuff: the trade-off between membrane permeability and selectivity. *Science* 356:eaab0530
9. Tang CY, Zhao Y, Wang R, Hélix-Nielsen C, Fane AG. 2012. Desalination by biomimetic aquaporin membranes: review of status and prospects. *Desalination* 308:34–40
10. Hélix-Nielsen C. 2018. Biomimetic membranes as a technology platform: challenges and opportunities. *Membranes* 8:e44
11. Fu Y, Jiang YB, Dunphy D, Xiong H, Coker E, et al. 2018. Ultra-thin enzymatic liquid membrane for CO₂ separation and capture. *Nat. Commun.* 9:990
12. Doyle D, Morais-Cabral J, Pfuetzner RA, Kuo A, Gulbis JM, et al. 1998. The structure of the potassium channel: molecular basis of K⁺ conduction and selectivity. *Science* 280:69–77
13. Zhou Y, Morais-Cabral J, Kaufman A, MacKinnon R. 2001. Chemistry of ion coordination and hydration revealed by a K⁺ channel–Fab complex at 2.0 Å resolution. *Nature* 414:43–48
14. MacKinnon R. 2003. Minireview: Potassium channels. *FEBS Lett.* 555:62–65
15. MacKinnon R. 2004. Potassium channels and the atomic basis of selective ion conduction (Nobel Lecture). *Angew. Chem. Int. Ed.* 43:4265–77
16. Asthagiri D, Pratt LR, Paulaitis ME. 2006. Role of fluctuations in a snug-fit mechanism of KcsA channel selectivity. *J. Chem. Phys.* 125:24701
17. Jiang Y, MacKinnon R. 2000. The barium site in a potassium channel by X-ray crystallography. *J. Gen. Phys.* 115:269–72
18. Lam YL, Zeng W, Sauer D, Jiang Y. 2014. The conserved potassium channel filter can have distinct ion binding profiles: structural analysis of rubidium, cesium, and barium binding in NaK2K. *J. Gen. Phys.* 144:181–92
19. Piasta KN, Theobald DL, Miller C. 2011. Potassium-selective block of barium permeation through single KcsA channels. *J. Gen. Phys.* 138:421–36
20. Guo R, Zeng W, Cui H, Chen L, Ye S. 2014. Ionic interactions of Ba²⁺ blockades in the MthK K⁺ channel. *J. Gen. Phys.* 144:193–200
21. Rempe SB, Rogers DM, Jiang YB, Yang S, Leung K, et al. 2010. *Computational and experimental platform for understanding and optimizing water flux and salt rejection in nanoporous membranes*. Rep. SAND2010-6735, Sandia Natl. Lab., Albuquerque, NM
22. Rempe SB, Brinker CJ, Rogers DM, Jiang YB, Yang S. 2016. *Biomimetic membranes and methods of making biomimetic membranes*. US Patent 9,486,742
23. Pohorille A, Pratt LR. 2012. Is water the universal solvent for life? *Orig. Life Evol. Biosph.* 42:405–9
24. Rempe SB, Pratt LR, Hummer G, Kress JD, Martin RL, Redondo A. 2000. The hydration number of Li⁺ in liquid water. *J. Am. Chem. Soc.* 122:966–67
25. Pratt LR, Rempe SB. 1999. Quasi-chemical theory and implicit solvent models for simulations. *AIP Conf. Proc.* 492:172–201
26. Varma S, Rempe SB. 2006. Coordination numbers of alkali metal ions in aqueous solutions. *Biophys. Chem.* 124:192–99
27. Mason PE, Ansell S, Neilson G, Rempe SB. 2015. Neutron scattering studies of the hydration structure of Li⁺. *J. Phys. Chem. B* 119:2003–9
28. Varma S, Rempe SB. 2007. Tuning ion coordination architectures to enable selective partitioning. *Biophys. J.* 93:1093–99

29. Stevens MJ, Rempe SB. 2016. Ion-specific effects in carboxylate binding sites. *J. Phys. Chem. B* 120:12519–30
30. Chaudhari MI, Rempe SB. 2018. Strontium and barium in aqueous solution and a potassium channel binding site. *J. Chem. Phys.* 148:222831
31. Lockless S, Zhou M, MacKinnon R. 2007. Structural and thermodynamic properties of selective ion binding in a K⁺ channel. *PLoS Biol.* 5:e121
32. Payandeh J, Pfoh R, Pai EF. 2013. The structure and regulation of magnesium selective ion channels. *Biochim. Biophys. Acta Biomembr.* 1828:2778–92
33. Takeda H, Hattori M, Nishizawa T, Yamashita K, Shah STA, et al. 2014. Structural basis for ion selectivity revealed by high-resolution crystal structure of Mg²⁺ channel MgtE. *Nat. Commun.* 5:5374
34. Tang L, Gamal El-Din TM, Payandeh J, Martinez GQ, Heard TM, et al. 2014. Structural basis for Ca²⁺ selectivity of a voltage-gated calcium channel. *Nature* 505:56–61
35. Cuello LG, Cortes DM, Perozo E. 2017. The gating cycle of a K⁺ channel at atomic resolution. *eLife* 6:e28032
36. Kshatri AS, Gonzalez-Hernandez AJ, Giraldez T. 2018. Functional validation of Ca²⁺-binding residues from the crystal structure of the BK ion channel. *Biochim. Biophys. Acta Biomembr.* 1860:943–52
37. Tilegenova C, Cortes DM, Jahovic N, Hardy E, Hariharan P, et al. 2019. Structure, function, and ion-binding properties of a K⁺ channel stabilized in the 2,4-ion-bound configuration. *PNAS* 116:16829–34
38. Miller C. 1982. Coupling of water and ion fluxes in a K⁺-selective channel of sarcoplasmic reticulum. *Biophys. J.* 38:227–30
39. Alcayaga C, Cecchi X, Alvarez O, Latorre R. 1989. Streaming potential measurements in Ca²⁺-activated K⁺ channels from skeletal and smooth muscle: coupling of ion and water fluxes. *Biophys. J.* 55:367–71
40. Iwamoto M, Oiki S. 2011. Counting ion and water molecules in a streaming file through the open-filter structure of the K channel. *J. Neurosci.* 31:12180–88
41. Armstrong C. 2015. Packaging life: the origin of ion-selective channels. *Biophys. J.* 109:173–77
42. Roux B. 2005. Ion conduction and selectivity in K⁺ channels. *Annu. Rev. Biophys. Biomol. Struct.* 34:153–71
43. Valiyaveetil F, Leonetti M, Muir TW, MacKinnon R. 2006. Ion selectivity in a semisynthetic K⁺ channel locked in the conductive conformation. *Science* 314:1004–7
44. Varma S, Sabo D, Rempe SB. 2008. K⁺/Na⁺ selectivity in K channels and valinomycin: over-coordination versus cavity-size constraints. *J. Mol. Biol.* 376:13–22
45. Sabo D, Jiao D, Varma S, Pratt LR, Rempe SB. 2013. Case study of Rb⁺(aq), quasi-chemical theory of ion hydration, and the *no split occupancies* rule. *Annu. Rep. C Phys. Chem.* 109:266–78
46. Muralidharan A, Pratt LR, Chaudhari MI, Rempe SB. 2018. Quasi-chemical theory with cluster sampling from *ab initio* molecular dynamics: fluoride (F⁻) anion hydration. *J. Phys. Chem. A* 122:9806–12
47. Fulton JL, Heald SM, Badyal YS, Simonson JM. 2003. Understanding the effects of concentration on the solvation structure of Ca²⁺ in aqueous solution. I: The perspective on local structure from EXAFS and XANES. *J. Phys. Chem. A* 107:4688–96
48. Galib M, Baer MD, Skinner LB, Mundy CJ, Huthwelker T, et al. 2017. Revisiting the hydration structure of aqueous Na⁺. *J. Chem. Phys.* 146:84504
49. Glezakou VA, Chen Y, Fulton JL, Schenter GK, Dang LX. 2006. Electronic structure, statistical mechanical simulations, and EXAFS spectroscopy of aqueous potassium. *Theor. Chem. Acc.* 115:86–99
50. Kirchner B, di Dio PJ, Hutter J. 2012. Real-world predictions from *ab initio* molecular dynamics simulations. *Top. Curr. Chem.* 307:109–53
51. Lyubartsev AP, Laasonen K, Laaksonen A. 2001. Hydration of Li⁺ ion: an *ab initio* molecular dynamics simulation. *J. Chem. Phys.* 114:3120–26
52. Heuft JM, Meijer EJ. 2005. Density functional theory based molecular-dynamics study of aqueous fluoride solvation. *J. Chem. Phys.* 122:94501
53. Whitfield TW, Varma S, Harder E, Lamoureux G, Rempe SB, Roux B. 2007. Theoretical study of aqueous solvation of K⁺ comparing *ab initio*, polarizable, and fixed-charge models. *J. Chem. Theor. Comp.* 3:2068–82

54. Bankura A, Santra B, DiStasio RA Jr, Swartz CW, Klein ML, Wu X. 2015. A systematic study of chloride ion solvation in water using van der Waals inclusive hybrid density functional theory. *Mol. Phys.* 113:2842–54
55. Leśniewski M, Śmiechowski M. 2018. Inside the water wheel: intrinsic differences between hydrated tetraphenylphosphonium and tetraphenylborate ions. *J. Chem. Phys.* 149:171101
56. Sharma B, Chandra A. 2018. Nature of hydration shells of a polyoxy-anion with a large cationic centre: the case of iodate ion in water. *J. Comput. Chem.* 39:1226–35
57. Zhou L, Xu J, Xu L, Wu X. 2019. Importance of van der Waals effects on the hydration of metal ions from the Hofmeister series. *J. Chem. Phys.* 150:124505
58. Karmakar A. 2019. Ab initio molecular dynamics simulation of supercritical aqueous ionic solutions: spectral diffusion of water in the vicinity of Br^- and I^- ions. *J. Mol. Liq.* 279:306–16
59. Martinek T, Duboué-Dijon E, Timr Š, Mason PE, Baxová K, et al. 2018. Calcium ions in aqueous solutions: accurate force field description aided by ab initio molecular dynamics and neutron scattering. *J. Chem. Phys.* 148:222813
60. Rempe SB, Asthagiri D, Pratt LR. 2004. Inner shell definition and absolute hydration free energy of $\text{K}^+(\text{aq})$ on the basis of quasi-chemical theory and *ab initio* molecular dynamics. *Phys. Chem. Chem. Phys.* 6:1966–69
61. Chaudhari MI, Soniat M, Rempe SB. 2015. Octa-coordination and the aqueous Ba^{2+} ion. *J. Phys. Chem. B* 119:8746–53
62. Chaudhari MI, Pratt LR, Rempe SB. 2018. Utility of chemical computations in predicting solution free energies of metal ions. *Mol. Simul.* 44:110–16
63. Varma S, Rempe SB. 2010. Multibody effects in ion binding and selectivity. *Biophys. J.* 99:3394–401
64. Rossi M, Tkatchenko A, Rempe SB, Varma S. 2013. Role of methyl-induced polarization in ion binding. *PNAS* 110:12978–83
65. Muralidharan A, Pratt LR, Chaudhari MI, Rempe SB. 2019. Quasi-chemical theory for anion hydration and specific ion effects: $\text{Cl}^-(\text{Aq})$ versus $\text{F}^-(\text{Aq})$. *Chem. Phys. Lett.* 4:100037
66. Peschke M, Blades AT, Kebarle P. 1998. Hydration energies and entropies for Mg^{2+} , Ca^{2+} , Sr^{2+} , and Ba^{2+} from gas-phase ion–water molecule equilibria determinations. *J. Phys. Chem. A* 102:9978–85
67. Tissandier MD, Cowen KA, Feng WY, Gundlach E, Cohen MH, et al. 1998. The proton's absolute aqueous enthalpy and Gibbs free energy of solvation from cluster-ion solvation data. *J. Phys. Chem. A* 102:7787–94
68. Chaudhari MI, Rempe SB, Pratt LR. 2017. Quasi-chemical theory of $\text{F}^-(\text{aq})$: the “no split occupancies rule” revisited. *J. Chem. Phys.* 147:161728
69. Robertson WH, Johnson MA. 2003. Molecular aspects of halide ion hydration: the cluster approach. *Annu. Rev. Phys. Chem.* 54:173–213
70. Morais-Cabral J, Zhou Y, MacKinnon R. 2001. Energetic optimization of ion conduction rate by the K^+ selectivity filter. *Nature* 414:37–42
71. Gouaux E, MacKinnon R. 2005. Principles of selective ion transport in channels and pumps. *Science* 310:1461–65
72. Beckstein O, Biggin PC, Bond P, Bright JN, Domene C, et al. 2003. Ion channel gating: insights via molecular simulations. *FEBS Lett.* 555:85–90
73. Catterall WA. 2011. Voltage-gated calcium channels. *Cold Spring Harb. Perspect. Biol.* 3:a003947
74. Kratochvil HT, Carr JK, Matulef K, Li H, Maj M, et al. 2016. Instantaneous ion configurations in the K^+ configurations in the K^+ ion channel selectivity filter revealed by 2D IR spectroscopy. *Science* 353:1040–44
75. Last NB, Sun S, Pham MC, Miller C. 2017. Molecular determinants of permeation in a fluoride-specific ion channel. *eLife* 6:e31259
76. Shlosman I, Marinelli F, Faraldo-Gómez JD, Mindell JA. 2018. The prokaryotic $\text{Na}^+/\text{Ca}^{2+}$ exchanger NCX_Mj transports Na^+ and Ca^{2+} in a 3:1 stoichiometry. *J. Gen. Phys.* 150:51–65
77. Tong A, Petroff JT, Hsu FF, Schmidpeter PAM, Nimigean CM, et al. 2019. Direct binding of phosphatidylglycerol at specific sites modulates desensitization of a pentameric ligand-gated ion channel. *eLife* 8:e50766

78. Oster C, Hendricks K, Kopec W, Chevelkov V, Shi C, et al. 2019. The conduction pathway of potassium channels is water free under physiological conditions. *Sci. Adv.* 5:eaaw6756
79. Hodgkin AL, Keynes RD. 1955. The potassium permeability of a giant nerve fibre. *J. Physiol.* 128:61–88
80. Sather WA, McCleskey EW. 2003. Permeation and selectivity in calcium channels. *Annu. Rev. Physiol.* 65:133–59
81. Dang TX, McCleskey EW. 1998. Ion channel selectivity through stepwise changes in binding affinity. *J. Gen. Physiol.* 111:185–93
82. Ohtomo N, Arakawa K. 1980. Neutron diffraction study of aqueous ionic solutions. II. Aqueous solutions of sodium chloride and potassium chloride. *Bull. Chem. Soc. Jpn.* 53:1789–94
83. Mason PE, Sullivan D, Neilson G, Ramos S. 2001. Neutron and X-ray scattering studies of hydration in aqueous solutions. *Philos. Trans. R. Soc. A* 359:1575–91
84. Soper AK, Weckström K. 2006. Ion solvation and water structure in potassium halide aqueous solutions. *Biophys. Chem.* 124:180–91
85. Mancinelli R, Botti A, Bruni F, Ricci MA, Soper AK. 2007. Hydration of sodium, potassium, and chloride ions in solution and the concept of structure maker/breaker. *J. Phys. Chem. B* 111:13570–77
86. Eisenman G, Horn R. 1983. The role of kinetic and equilibrium processes in ion permeation through channels. *J. Membr. Biol.* 76:197–225
87. Collins KD. 1997. Density-dependent strength of hydration and biological structure. *Biophys. J.* 72:65–76
88. Varma S, Rogers DM, Pratt LR, Rempe SB. 2011. Design principles for K⁺ selectivity in membrane transport. *J. Gen. Phys.* 137:479–88
89. Armstrong CM, Taylor SR. 1980. Interaction of barium ions with potassium channels in squid giant axons. *Biophys. J.* 30:473–88
90. Armstrong CM, Swenson RP, Taylor SR. 1982. Block of squid axon K-channels by internally and externally applied barium ions. *J. Gen. Phys.* 80:663–82
91. Neupert-Laves K, Dobler M. 1975. The crystal structure of a K⁺ complex of valinomycin. *Helv. Chim. Acta* 58:432–42
92. Bhate MP, Wylie BJ, Tian L, McDermott AE. 2010. Conformational dynamics in the selectivity filter of KcsA in response to potassium ion concentration. *J. Mol. Biol.* 401:155–66
93. Noskov SY, Bernèche S, Roux B. 2004. Control of ion selectivity in potassium channels by electrostatic and dynamic properties of carbonyl ligands. *Nature* 431:830–34
94. Rogers DM, Jiao D, Pratt L, Rempe SB. 2012. Structural models and molecular thermodynamics of hydration of ions and small molecules. *Annu. Rep. Comput. Chem.* 8:71–127
95. Verkhatsky A, Parpura V. 2014. Calcium signalling and calcium channels evolution and general principles. *Eur. J. Pharm.* 739:1–3
96. Carafoli E. 1987. Intracellular calcium homeostasis. *Annu. Rev. Biochem.* 56:395–433
97. Romani AMP. 2011. Cellular magnesium homeostasis. *Arch. Biochem. Biophys.* 512:1–23
98. Armstrong CM, Palti Y. 1991. Potassium channel block by internal calcium and strontium. *J. Gen. Phys.* 97:627–38
99. Elinder F, Madeja M, Arhem P. 1996. Surface charges of K channels. Effects of strontium on five cloned channels expressed in *Xenopus* oocytes. *J. Gen. Phys.* 108:325–32
100. Sugihara I. 1998. Activation and two modes of blockade by strontium of Ca²⁺-activated K⁺ channels in goldfish saccular-hair cells. *J. Gen. Physiol.* 111:363–79
101. Soh H, Park CS. 2002. Localization of divalent cation-binding site in the pore of a small conductance Ca²⁺-activated K⁺ channel and its role in determining current–voltage relationship. *Biophys. J.* 83:2528–38
102. Asthagiri D, Dixit P, Merchant S, Paulaitis M, Pratt L, et al. 2010. Ion selectivity from local configurations of ligands in solutions and ion channels. *Chem. Phys. Lett.* 485:1–7
103. Rogers DM, Rempe SB. 2011. Probing the thermodynamics of competitive ion binding using minimum energy structures. *J. Phys. Chem. B* 115:9116–29
104. Asthagiri D, Pratt LR, Paulaitis ME, Rempe SB. 2004. Hydration structure and free energy of biomolecularly specific aqueous dications, including Zn²⁺ and first transition row metals. *J. Am. Chem. Soc.* 126:1285–89

105. Asthagiri D, Pratt LR, Ashbaugh HS. 2003. Absolute hydration free energies of ions, ion–water clusters, and quasichemical theory. *J. Chem. Phys.* 119:2702–8
106. Jiao D, Rempe SB. 2012. Combined density functional theory (DFT) and continuum calculations of pK_a in carbonic anhydrase. *Biochemistry* 51:5979–89
107. Dudev T, Lim C. 2013. Importance of metal hydration on the selectivity of Mg^{2+} versus Ca^{2+} in magnesium ion channels. *J. Am. Chem. Soc.* 135:17200–8
108. Beck TL, Paulaitis ME, Pratt LR. 2006. *The Potential Distribution Theorem and Models of Molecular Solutions*. Cambridge, UK: Cambridge Univ. Press
109. Shah J, Asthagiri D, Pratt L, Paulaitis M. 2007. Balancing local order and long-ranged interactions in the molecular theory of liquid water. *J. Chem. Phys.* 127:144508
110. Kebarle P. 1977. Ion thermochemistry and solvation from gas phase ion equilibria. *Annu. Rev. Phys. Chem.* 28:445–76
111. Keesee RG, Castleman AW Jr. 1980. Gas-phase studies of hydration complexes of Cl^- and I^- and comparison to electrostatic calculations in the gas phase. *Chem. Phys. Lett.* 74:139–42
112. Keesee RG, Lee N, Castleman AW Jr. 1980. Properties of clusters in the gas phase. V. Complexes of neutral molecules onto negative ions. *J. Chem. Phys.* 73:2195–202
113. Castleman AW Jr., Keesee RG. 1986. Ionic clusters. *Chem. Rev.* 86:589–618
114. Castleman AW Jr., Keesee RG. 1988. Gas-phase clusters: spanning the states of matter. *Science* 241:36–42
115. Tomasi J, Mennucci B, Cammi R. 2005. Quantum mechanical continuum solvation models. *Chem. Rev.* 105:2999–3093
116. Pethica BA. 2007. Are electrostatic potentials between regions of different chemical composition measurable? The Gibbs–Guggenheim principle reconsidered, extended and its consequences revisited. *Phys. Chem. Chem. Phys.* 9:6253–62
117. Landau LD, Lifshitz EM. 1960. *Course in Theoretical Physics*, Vol. 8. New York: Pergamon
118. Zhou Y, Stell G, Friedman HL. 1988. Note on standard free energy of transfer and partitioning of ionic species between two fluid phases. *J. Chem. Phys.* 89:3836–39
119. Nichols AL, Pratt LR. 1984. Salt effects on the surface tensions of dilute electrolyte solutions: the influence of nonzero relative solubility of the salt between the coexisting phases. *J. Chem. Phys.* 80:6225–33
120. Pratt LR. 1992. Contact potentials of solution interfaces: phase equilibrium and interfacial electric fields. *J. Phys. Chem* 96:25–33
121. You X, Chaudhari MI, Pratt LR. 2014. Comparison of mechanical and thermodynamical evaluations of electrostatic potential differences between electrolyte solutions. In *Aqua Incognita: Why Ice Floats on Water and Galileo 400 Years On*, ed. P Lo Nostro, BW Ninham, pp. 434–42. Ballarat, Aust.: Connor Court
122. Lyklema J. 2017. View of interfacial potentials: measuring the immeasurable? *Substantia* 1:75–93
123. Beck TL. 2013. The influence of water interfacial potentials on ion hydration in bulk water and near interfaces. *Chem. Phys. Lett.* 561/562:1–13
124. Pollard TP, Beck TL. 2018. Re-examining the tetraphenyl-arsonium/tetraphenyl-borate (TATB) hypothesis for single-ion solvation free energies. *J. Chem. Phys.* 148:222830
125. Doyle C, Shi Y, Beck TL. 2019. The importance of the water molecular quadrupole for estimating interfacial potential shifts acting on ions near the liquid-vapor interface. *J. Phys. Chem. B* 123:3348–58
126. Marcus Y. 1987. The thermodynamics of solvation of ions. Part 4. Application of the tetraphenylarsonium tetraphenylborate (TATB) extrathermodynamic assumption to the hydration of ions and to properties of hydrated ions. *J. Chem. Soc.* 83:2985–92
127. Schurhammer R, Wipff G. 2000. Are the hydrophobic $AsPh_4^+$ and BPh_4^- ions equally solvated? A theoretical investigation in aqueous and nonaqueous solutions using different charge distributions. *J. Phys. Chem. A* 104:11159–68
128. Duignan TT, Baer MD, Mundy CJ. 2018. Understanding the scale of the single ion free energy: a critical test of the tetra-phenyl arsonium and tetra-phenyl borate assumption. *J. Chem. Phys.* 148:222819
129. Leung K, Rempe SB, von Lilienfeld OA. 2009. *Ab initio* molecular dynamics calculations of ion hydration free energies. *J. Chem. Phys.* 130:204507
130. Marcus Y. 1994. A simple empirical model describing the thermodynamics of hydration of ions of widely varying charges, sizes, and shapes. *Biophys. Chem.* 51:111–27

131. Friedman H, Krishnan C. 1973. Thermodynamics of ionic hydration. In *Water, a Comprehensive Treatise*, Vol. 3: *Aqueous Solutions of Simple Electrolytes*, ed. F Franks, pp. 1–118. Berlin: Springer
132. Marcus Y. 2015. *Ions in Solution and Their Solvation*. New York: Wiley
133. Hummer G. 2014. Potassium ions line up. *Science* 346:303
134. Kopec W, de Groot BL. 2019. Molecular simulations of ion permeation, gating and selectivity in K^+ channels. *Biophys. J.* 116:16a
135. Jiao D, King C, Grossfield A, Darden TA, Ren P. 2006. Simulation of Ca^{2+} and Mg^{2+} solvation using polarizable atomic multipole potential. *J. Phys. Chem. B* 110:18553–59
136. Mehandzhyski AY, Riccardi E, van Erp TS, Trinh TT, Grimes BA. 2015. Ab initio molecular dynamics study on the interactions between carboxylate ions and metal ions in water. *J. Phys. Chem. B* 119:10710–19
137. Soniat M, Hartman L, Rick SW. 2015. Charge transfer models of zinc and magnesium in water. *J. Chem. Theory Comput.* 11:1658–67
138. Mazur S. 1992. Neighborhood partition of the radial distribution function for simple liquids. *J. Chem. Phys.* 97:9276–82
139. Zhu P, You X, Pratt L, Papadopoulos K. 2011. Generalizations of the Fuoss approximation for ion pairing. *J. Chem. Phys.* 134:54502
140. Dudev T, Cowan JA, Lim C. 1999. Competitive binding in magnesium coordination chemistry: water versus ligands of biological interest. *J. Am. Chem. Soc.* 121:7665–73
141. Caminiti R, Licheri G, Piccaluga G, Pinna G. 1979. X-ray diffraction study of $MgCl_2$ aqueous solutions. *J. Appl. Cryst.* 12:34–38
142. Harris DJ, Brodholt JP, Sherman DM. 2003. Hydration of Sr^{2+} in hydrothermal solutions from *ab initio* molecular dynamics. *J. Phys. Chem. B* 107:9056–58
143. Spohr E, Palinkas G, Heinzinger K, Bopp P, Probst MM. 2002. Molecular dynamics study of an aqueous strontium chloride solution. *J. Phys. Chem.* 92:6754–61
144. Ohtaki H, Radnai T. 1993. Structure and dynamics of hydrated ions. *Chem. Rev.* 93:1157–204
145. Bernal JD, Fowler RH. 1933. A theory of water and ionic solution, with particular reference to hydrogen and hydroxyl ions. *J. Chem. Phys.* 1:515–48
146. Alam TM, Hart D, Rempe SB. 2011. Computing the 7Li NMR chemical shielding of hydrated Li^+ using cluster calculations and time-averaged configurations from *ab-initio* molecular dynamics simulations. *Phys. Chem. Chem. Phys.* 13:13629–37
147. Caminiti R, Licheri G, Piccaluga G, Pinna G. 1977. X-ray diffraction study of a “three-ion” aqueous solution. *Chem. Phys. Lett.* 47:275–78
148. Licheri G, Piccaluga G, Pinna G. 1975. X-ray diffraction study of $CaBr_2$ aqueous solutions. *J. Chem. Phys.* 63:4412–14
149. Ramos S, Neilson GW, Barnes AC. 2003. Anomalous X-ray diffraction studies of Sr^{2+} hydration in aqueous solution. *J. Chem. Phys.* 118:5542–46
150. Pfund DM, Darab JG, Fulton JL, Ma Y. 2002. An XAFS study of strontium ions and krypton in supercritical water. *J. Phys. Chem.* 98:13102–7
151. Ramos S, Barnes AC, Neilson GW, Capitan MJ. 2000. Anomalous X-ray diffraction studies of hydration effects in concentrated aqueous electrolyte solutions. *Chem. Phys.* 258:171–80
152. D’Angelo P, Pavel N, Roccatano D, Nolting HF. 1996. Multielectron excitations at the L edges of barium in aqueous solution. *Phys. Rev. B* 54:12129–38
153. Linder B, Hoernschemeyer D. 1967. Cavity concept in dielectric theory. *J. Chem. Phys.* 46:784–90
154. Wilson MA, Wei C, Bjelkmar P, Wallace BA, Pohorille A. 2011. Molecular dynamics simulation of the antimioebin ion channel: linking structure and conductance. *Biophys. J.* 100:2394–402

Contents

Spatially Resolved Exciton and Charge Transport in Emerging Semiconductors <i>Naomi S. Ginsberg and William A. Tisdale</i>	1
Accelerated Reaction Kinetics in Microdroplets: Overview and Recent Developments <i>Zhenwei Wei, Yangjie Li, R. Graham Cooks, and Xin Yan</i>	31
Biomolecular Phase Separation: From Molecular Driving Forces to Macroscopic Properties <i>Gregory L. Dignon, Robert B. Best, and Jeetain Mittal</i>	53
Roaming Reactions and Dynamics in the van der Waals Region <i>Arthur G. Suits</i>	77
Chromatosome Structure and Dynamics from Molecular Simulations <i>Mehmet Ali Öztürk, Madhura De, Vlad Cojocaru, and Rebecca C. Wade</i>	101
The Exploration of Chemical Reaction Networks <i>Jan P. Unsleber and Markus Reiher</i>	121
High-Field Dynamic Nuclear Polarization <i>Björn Corzilius</i>	143
Molecular Simulations of Gram-Negative Bacterial Membranes Come of Age <i>Wonpil Im and Syma Khalid</i>	171
Benchmark Experimental Gas-Phase Intermolecular Dissociation Energies by the SEP-R2PI Method <i>Richard Knochenmuss, Rajeev K. Sinha, and Samuel Leutwyler</i>	189
The Maximum Caliber Variational Principle for Nonequilibria <i>Kingsbuk Ghosh, Purushottam D. Dixit, Luca Agozzino, and Ken A. Dill</i>	213
Mapping Structural Dynamics of Proteins with Femtosecond Stimulated Raman Spectroscopy <i>Chong Fang and Longteng Tang</i>	239

Low-Frequency Protein Motions Coupled to Catalytic Sites <i>Christopher M. Cheatum</i>	267
Nonstatistical Reaction Dynamics <i>Bhumika Jayee and William L. Hase</i>	289
Photoemission from Free Particles and Droplets <i>Loren Ban, Bruce L. Yoder, and Ruth Signorell</i>	315
Electron Transfer from Semiconductor Nanocrystals to Redox Enzymes <i>James K. Utterback, Jesse L. Ruzicka, Helena R. Keller, Lauren M. Pellows, and Gordana Dukovic</i>	335
Machine Learning for Molecular Simulation <i>Frank Noé, Alexandre Tkatchenko, Klaus-Robert Müller, and Cecilia Clementi</i>	361
Single-Molecule FRET of Intrinsically Disordered Proteins <i>Lauren Ann Metskas and Elizabeth Rhoades</i>	391
Excited-State Imaging of Single Particles on the Subnanometer Scale <i>Alison Wallum, Huy A. Nguyen, and Martin Gruebele</i>	415
Bose–Einstein Condensation of Exciton-Polaritons in Organic Microcavities <i>Jonathan Keeling and Stéphane Kéna-Cohen</i>	435
Hydration Mimicry by Membrane Ion Channels <i>Mangesh I. Chaudhari, Juan M. Vanegas, L.R. Pratt, Ajay Muralidharan, and Susan B. Rempe</i>	461

Errata

An online log of corrections to *Annual Review of Physical Chemistry* articles may be found at <http://www.annualreviews.org/errata/physchem>